JACS
JOURNAL OF THE AMERICAN CHEMICAL SOCIETY
Article
pubs.acs.org/JACS

Characterization of Porphyrin-Co(III)-'Nitrene Radical' Species Relevant in Catalytic Nitrene Transfer Reactions

Monalisa Goswami,[†,▽] Volodymyr Lyaskovskyy,[†,▽] Sérgio R. Domingos,[‡] Wybren Jan Buma,[‡] Sander Woutersen,[‡] Oliver Troeppner,[§] Ivana Ivanović-Burmazović,[§] Hongjian Lu,[⊥] Xin Cui,[⊥] X. Peter Zhang,*[,⊥] Edward J. Reijerse,[∥] Serena DeBeer,[∥] Matti M. van Schooneveld,[∥] Florian Felix Pfaff,[#] Kallol Ray,[#] and Bas de Bruin*[,†]

[†]Van 't Hoff Institute for Molecular Sciences (HIMS), Homogeneous and Supramolecular Catalysis and [‡]HIMS, Photonics group, University of Amsterdam, Science Park 904, 1098 XH Amsterdam, The Netherlands

[§]Lehrstuhl für Bioanorganische Chemie, Department Chemie und Pharmazie, Universität Erlangen-Nürnberg. Egerlandstraße 1, D-91058 Erlangen, Germany

[⊥]Department of Chemistry, University of South Florida, Tampa, Florida 33620-5250, United States

[∥]Max Planck Institut für Chemische Energiekonversion, Stiftstraße 34-36, 45470 Mülheim an der Ruhr, Germany

[#]Institut für Chemie, Humboldt-Universität zu Berlin, Brook-Taylor-Straße 2, 12489 Berlin, Germany

Supporting Information

ABSTRACT: To fully characterize the Co^{III}–'nitrene radical' species that are proposed as intermediates in nitrene transfer reactions mediated by cobalt(II) porphyrins, different combinations of cobalt(II) complexes of porphyrins and nitrene transfer reagents were combined, and the generated species were studied using EPR, UV–vis, IR, VCD, UHR-ESI-MS, and XANES/XAFS measurements. Reactions of cobalt(II) porphyrins $\mathbf{1}^{\mathbf{P1}}$ (**P1** = *meso*-tetraphenylporphyrin (TPP)) and $\mathbf{1}^{\mathbf{P2}}$ (**P2** = 3,5-Di^{t}Bu-ChenPhyrin) with organic azides $\mathbf{2}_{\mathbf{Ns}}$ (NsN_3), $\mathbf{2}_{\mathbf{Ts}}$ (TsN_3), and $\mathbf{2}_{\mathbf{Troc}}$ ($TrocN_3$) led to the formation of mono-nitrene species $\mathbf{3}^{\mathbf{P1}}{}_{\mathbf{Ns}}$, $\mathbf{3}^{\mathbf{P2}}{}_{\mathbf{Ts}}$, and $\mathbf{3}^{\mathbf{P2}}{}_{\mathbf{Troc}}$, respectively, which are best described as $[Co^{III}(por)(NR''^{\bullet-})]$ nitrene radicals (imidyl radicals) resulting from single electron transfer from the cobalt(II) porphyrin to the 'nitrene' moiety (Ns: R″ = $-SO_2$-*p*-$C_6H_5NO_2$; Ts: R″ = $-SO_2C_6H_6$; Troc: R″ = $-C(O)OCH_2CCl_3$). Remarkably, the reaction of $\mathbf{1}^{\mathbf{P1}}$ with *N*-nosyl iminoiodane (PhI═NNs) $\mathbf{4}_{\mathbf{Ns}}$ led to the formation of a bis-nitrene species $\mathbf{5}^{\mathbf{P1}}{}_{\mathbf{Ns}}$. This species is best described as a triple-radical complex $[(por^{\bullet-})Co^{III}(NR''^{\bullet-})_2]$ containing three ligand-centered unpaired electrons: two nitrene radicals ($NR''^{\bullet-}$) and one oxidized porphyrin radical ($por^{\bullet-}$). Thus, the formation of the second nitrene radical involves another intramolecular one-electron transfer to the "nitrene" moiety, but now from the porphyrin ring instead of the metal center. Interestingly, this bis-nitrene species is observed only on reacting $\mathbf{4}_{\mathbf{Ns}}$ with $\mathbf{1}^{\mathbf{P1}}$. Reaction of the more bulky $\mathbf{1}^{\mathbf{P2}}$ with $\mathbf{4}_{\mathbf{Ns}}$ results again in formation of mainly mono-nitrene species $\mathbf{3}^{\mathbf{P2}}{}_{\mathbf{Ns}}$ according to EPR and ESI-MS spectroscopic studies. The mono- and bis-nitrene species were initially expected to be five- and six-coordinate species, respectively, but XANES data revealed that both mono- and bis-nitrene species are six-coordinate O_h species. The nature of the sixth ligand bound to cobalt(III) in the mono-nitrene case remains elusive, but some plausible candidates are NH_3, NH_2^-, $NsNH^-$, and OH^-; $NsNH^-$ being the most plausible. Conversion of mono-nitrene species $\mathbf{3}^{\mathbf{P1}}{}_{\mathbf{Ns}}$ into bis-nitrene species $\mathbf{5}^{\mathbf{P1}}{}_{\mathbf{Ns}}$ upon reaction with $\mathbf{4}_{\mathbf{Ns}}$ was demonstrated. Solutions containing $\mathbf{3}^{\mathbf{P1}}{}_{\mathbf{Ns}}$ and $\mathbf{5}^{\mathbf{P1}}{}_{\mathbf{Ns}}$ proved to be still active in catalytic aziridination of styrene, consistent with their proposed key involvement in nitrene transfer reactions mediated by cobalt(II) porphyrins.

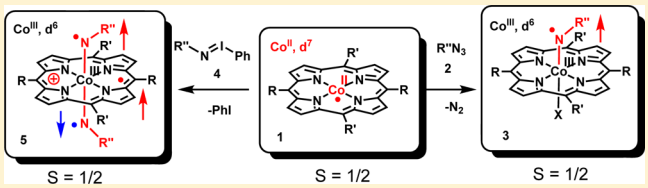

INTRODUCTION

Catalytic functionalization of C–H bonds is a desirable tool in organic and organometallic chemistry, as it is an atom-, time-, and cost-efficient alternative to traditional hydrocarbon functionalization.[1−3] Therefore, C–H insertion of carbenoid and nitrenoid species has emerged as a very promising protocol in the recent years.[4,5] The insertion of metal carbenoids into C–H bonds is now a well-established transformation, and many transition-metal catalysts that can catalyze such reactions have been disclosed in the past decade.[4,6,7] In addition to catalytic cyclopropanation and C–H insertion, metal-catalyzed carbene transfer has also made it possible to perform insertions into X–H bonds (X = O, N, S, Si) and to convert alkynes to cyclopropenes (including some cycloaddition reactions).[4] Given the ubiquity of nitrogen atoms in biologically active compounds,[8] nitrene transfer reactions also have very important applications in making molecules of interest. However, the applicability of metal-nitrenoids has so far been

Received: February 3, 2015
Published: April 6, 2015

DOI: 10.1021/jacs.5b01197
J. Am. Chem. Soc. 2015, 137, 5468−5479

limited to alkene aziridination,[9,10] C−H amination[11,12] and amidation.[13]

Among several catalysts that have been reported for nitrene transfer reactions, the most successful ones are still based on non-abundant Rh[4−6,13−17] and Ru[4,6,7,18−20] metals. Among the first row transition metals, there have been reports of Mn,[21,22] Cu,[23−26] and Fe[27] catalyzed systems. Besides being very efficient in carbene transfer reactions,[28−31] cobalt(II) porphyrin catalysts have also attracted attention in nitrene transfer reactions. Until the early 2000s, it was quite common to use iminoiodanes[32−36] or haloamine-T[23,25,26] compounds as nitrene sources. These are, however, not the most benign nitrene sources as they lead to the formation of undesirable side products like phenyl iodide and other halogen-containing compounds. With the efforts of various groups, organic azides[37,38] were discovered to be potentially greener resources to transfer nitrenes, as the only byproduct formed during the generation of nitrenes from azides is dinitrogen. The other disadvantage of using iminoiodanes is their poor solubility and the fact that there is not much scope to change the pre-existing functionality on the nitrogen atom.

With the use of differently meso-substituted cobalt(II) porphyrins ($\mathbf{1}^{P1}$−$\mathbf{1}^{P4}$ in Figure 1) a variety of nitrene transfer

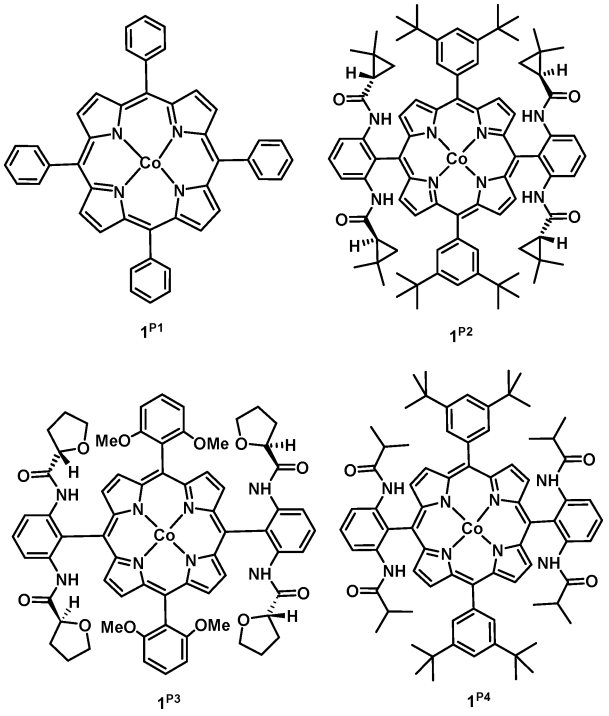

Figure 1. Commonly used cobalt(II) porphyrins in nitrene transfer reactions.

reagents (Figure 2) have been employed. For example, with the use of reagents like diphenyl phosphoryl azide (DPPA),[39,40] it is possible to further modify the substituent, as the nitrogen−phosphorus bond in the product aziridine is readily hydrolyzed. In the pursuit of finding more nitrene transfer reagents with easily removable groups on the nitrogen atom, trichloroethoxysulfonyl azide[41] ($TcesN_3$, Tces = trichloroethoxysulfonyl = $CCl_3CH_2O(SO_2)$−) was found to be effective. Apart from the nitrene precursors itself, specially tailored cobalt porphyrins, for example, with H-bonding functionalities, have further enhanced the applicability of these systems (see Figure 1; **P1** = *meso*-

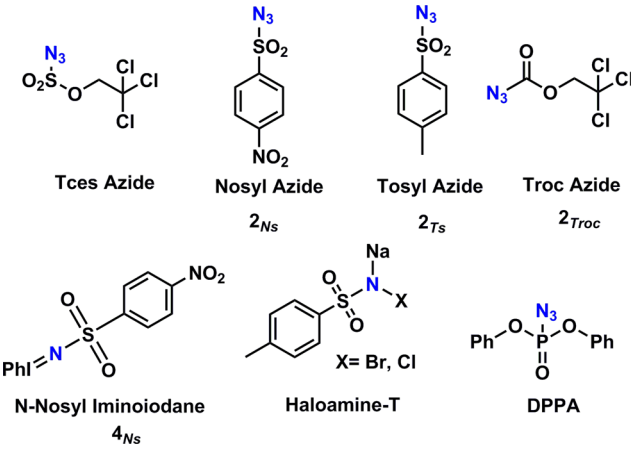

Figure 2. Commonly used nitrene transfer reagents.

tetraphenylporphyrin, **P2** = 3,5-di^{t}Bu-ChenPhyrin; **P3** = 2,6-diMeO-ZhuPhyrin; **P4** = 3,5-di^{t}Bu-IbuPhyrin). With the use of $\mathbf{1}^{P4}$, organic azides like tosyl azide can also be used as a viable nitrene source. H-bonding interactions between the nitrene moiety and the arms of the catalyst $\mathbf{1}^{P4}$ facilitate nitrenoid formation[42] and lead to an increased catalyst efficiency and lifetime. Enantioselective aziridination of alkenes was reported a few years ago using chiral cobalt(II)-porphyrin $\mathbf{1}^{P3}$ with $TcesN_3$, and enantioselectivity of 99% could be obtained.[41]

The mechanistic aspects of two such catalytic nitrene transfer reactions with cobalt porphyrins have been elucidated by our groups previously (Scheme 1).[9,43] The mechanism of C−H

Scheme 1. (a) DFT-Calculated Mechanism of Co(II) Porphyrin-Mediated Benzylic C−H Amination of Ethylbenzene by $N_3C(O)OMe$ and (b) Co(II) Porphyrin-Mediated Aziridination of Styrene with $PhSO_2N_3$

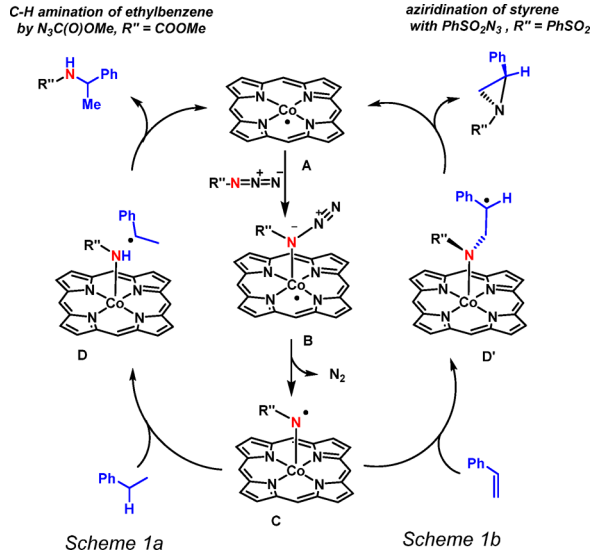

bond amination of ethylbenzene, toluene, and 1,2,3,4-tetrahydronaphthalene (tetralin) using a series of different organic azides ($N_3C(O)OMe$, N_3SO_2Ph, $N_3C(O)Ph$ and $N_3P(O)(OMe)_2$) as nitrene sources was studied using density functional theory (DFT) and electron paramagnetic resonance (EPR) spectroscopy (Scheme 1a).[43] The mechanism of cobalt(II) porphyrin-mediated aziridination of styrene with $PhSO_2N_3$ was also studied (Scheme 1b).[9] For both amination

DOI: 10.1021/jacs.5b01197
J. Am. Chem. Soc. 2015, 137, 5468−5479

and aziridination reactions, the DFT calculations revealed a stepwise radical process involving coordination of the azide to the cobalt(II) center, followed by release of dinitrogen to produce an unusual 'nitrene radical' intermediate **C** (Scheme 1). In addition, experimental EPR spectroscopic studies, combined with DFT calculated EPR properties being in good agreement with the experimental data, revealed the formation of a (por)Co^{III}–$N^{\bullet}$Y nitrene radical adduct **C** from the catalyst in the presence of an excess of the azide in benzene. Formation of a nitrene moiety at cobalt(II) effectively leads to electron transfer from the metal to the nitrene, thus reflecting the redox non-innocence of the nitrene ligand. The spin density of this intermediate resides almost entirely on the nitrogen atom of the nitrene moiety. A simplified molecular orbital picture showing the frontier π-interactions and explaining the unusual electronic structure of this intermediate is depicted in Scheme 2.

Scheme 2. Redox Non-Innocent Behaviour of Nitrene Ligands Coordinated to Open-Shell Co^{II}(por) Species (A), a Simplified Bonding Scheme Explaining This Behavior (B), and Alternative Bonding Scheme Involving a Triplet Nitrene (C)

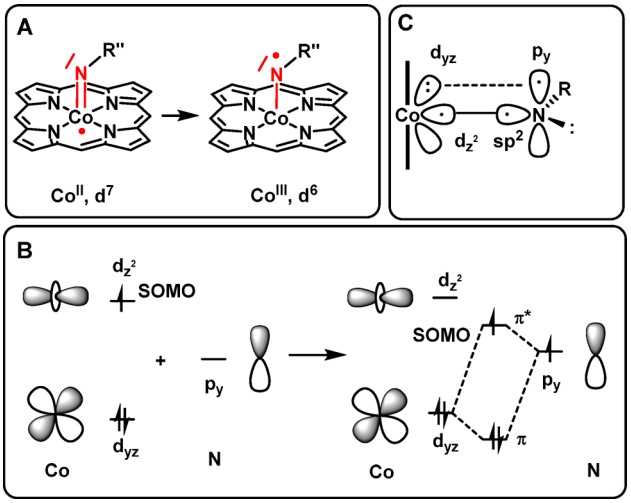

Experimental detection of these radicaloid species led us to investigate the subsequent stepwise C–H amination sequence computationally. According to these investigations, the amination reaction follows a stepwise radical pathway, in which the nitrene radical intermediate **C** readily abstracts a hydrogen atom from the benzylic position of the organic substrate. This leads to formation of a close-contact pair (**D**) of the thus-formed organic radical R′$^{\bullet}$ and the $cobalt^{III}$–amido complex (por)Co^{III}–NHR′′. Subsequent back-attack of the organic radical onto the amido moiety in **D**, in a rebound-type mechanism, leads to release of the desired amine products with regeneration of the cobalt(II) catalyst, which proceeds with low activation barriers according to DFT.

Nitrene transfer to styrene also proceeds in a stepwise manner via radical addition of the nitrene radical **C** to the C=C double bond of styrene to form γ-alkyl radical intermediates **D**′ (Scheme 1b). The cobalt(III) ion in **D**′ has an intermediate (S = 1) spin-state with its unpaired electrons antiferromagnetically coupled to the unpaired electron of the γ-alkyl radical, thus explaining its overall doublet (S = 1/2) state. Species **D**′ easily collapses in an almost barrierless ring closure reaction to form the aziridine, thereby regenerating the cobalt(II) porphyrin catalyst. Additionally, the computed free energy profile well explained the superior performance of the reported Co^{II}(porAmide) system $\mathbf{1}^{P4}$ with H-bond donor functionalities over the non-functionalized system $\mathbf{1}^{P1}$ (see Figure 2).[42]

Thus, the DFT calculations and the X-band EPR data gathered thus far strongly indicate the formation of substrate-centered (por)Co^{III}–$N^{\bullet}$–R″ nitrene radicals, which are proposed to be key intermediates in the mechanisms of the catalytic C–H amination and alkene aziridination reactions mediated by Co^{II}(por) catalysts and employing organic azides as nitrene sources. These nitrene radicals have thus far only been detected by means of X-band EPR spectroscopy.[9,43] Here we disclose their detection and characterization with a variety of spectroscopic and mass spectrometric techniques.

Ligand-centered radical complexes play a pivotal role in a number of bio- and "bioinspired" catalytic transformations, providing a powerful tool to control the reactivity and selectivity of the catalyst.[44−46] Such species are well-studied and characterized for transition-metal complexes containing typical polydentate redox non-innocent ligands, such as semi quinone-type radical ligands[47−49] and their nitrogen analogs,[47−50] reduced bipyridine and terpyridine ligands,[51−53] α-iminopyridine ligands,[54−56] and pyridine-2,6-diimine ligands.[57−61] More recently, considerable efforts have been made to understand the (electronic) structure and reactivity of monodentate redox non-innocent substrate-type ligands, such as carbenes,[62] which play a key role in catalytic carbene transfer reactions.[63,64] So far, only a few examples have been reported in which complexes bearing monodentate nitrogen-based radicaloid ligands were experimentally detected. Thus, well-studied complexes with redox active aminyl ligand radicals are limited to only a few well-characterized examples,[65] and related complexes bearing redox non-innocent nitrene ligands are even scarcer.[9,43,65−67] Given the importance of these radicaloid nitrene species in metal-catalyzed nitrene transfer and C–H functionalization reactions,[10,12,13,39−42,68] we gathered more experimental evidence for the formation of the previously reported mono-nitrene radical complexes upon reaction of cobalt(II) porphyrins with nitrene transfer reagents.[9,43] Furthermore, we here reveal the first example of a bis-nitrene species of $\mathbf{1}^{P1}$ upon reacting the stronger oxidizing nitrene transfer agent *N*-nosyl iminoiodane $\mathbf{4}_{Ns}$ with $\mathbf{1}^{P1}$. This bis-nitrene species has a markedly different electronic structure than the previously detected mono-nitrene species and also differs from the electronic structure of the previously reported diamagnetic bis-imido Ru^{VI}-porphyrin species (por)Ru^{VI}((=NR′′)$_2$).[69−73] The work described herein further bears some similarity with the mono- and bis-nitrene species of non-heme iron complexes disclosed by Che and co-workers,[66] but again the electronic structures reported herein are entirely different.

RESULTS AND DISCUSSION

To study the key nitrene intermediates in nitrene transfer reactions mediated by cobalt(II) porphyrins, we chose to react a few of the commonly used nitrene sources with two different types of cobalt(II) porphyrins: the tetraphenyl-substituted porphyrin $\mathbf{1}^{P1}$ and the bulkier (and chiral) H-bond donor appended porphyrin $\mathbf{1}^{P2}$ (see Figure 1). Complex $\mathbf{1}^{P2}$ serves as a model system for all reported cases where Co^{II} porphyrins with H-bonding moieties were proven to give superior catalytic results and where H-bonding stabilizes the formed nitrene intermediates.[41,8] In total, four different nitrene sources were employed. As mentioned before, these sources are known in

DOI: 10.1021/jacs.5b01197
J. Am. Chem. Soc. 2015, 137, 5468−5479

literature to be active in different nitrene transfer reactions like aziridination and amination.[8−11] Three of these were organic azides $\mathbf{2}_{Ns}$, $\mathbf{2}_{Ts}$, and $\mathbf{2}_{Troc}$ (see Figure 2): Nosyl azide ($\mathbf{2}_{Ns}$; NsN_3; Ns = Nosyl = *p*-NO_2−$PhSO_2$−), Tosyl azide ($\mathbf{2}_{Ts}$; TsN_3; Ts = Tosyl = *p*-$MePhSO_2$−), and Troc azide ($\mathbf{2}_{Troc}$; $TrocN_3$; Troc =2,2,2-trichlorethoxycarbonyl = CCl_3CH_2O-(CO)−). The fourth nitrene transfer reagent investigated was the stronger oxidizing *N*-nosyl iminoiodane (PhI═NNs) $\mathbf{4}_{Ns}$. To perform the EPR, ultra high-resolution electron spray ionization mass spectrometry (UHR-ESI), UV−vis, and X-ray absorption spectroscopy (XAS) studies, the following method was employed: To a solution of the catalyst in benzene-d_6 we added a 100-fold excess of the nitrene precursor. The catalyst concentrations of these solutions were typically 2.5 mM. The solvent used was benzene-d_6 in all cases, and this was chosen to avoid any cases of C−H insertions as is known for these systems in toluene, cyclohexane, and other related solvents.[10,11] Unless mentioned otherwise, deuterated benzene was chosen as the solvent to further slow down any C−H activation of the benzene ring itself.

EPR Spectroscopy of the Mono-Nitrene Species. Upon reaction of $\mathbf{1}^{P1}$ with a 100-fold excess of $\mathbf{2}_{Ns}$ and $\mathbf{1}^{P2}$ with a 100-fold excess of either $\mathbf{2}_{Ts}$ or $\mathbf{2}_{Troc}$ (Scheme 3), clear gradual changes in the X-band EPR spectra occurred that point to the formation of mono-nitrene radical species, revealing the redox non-innocence of the nitrene moiety. The disappearance of signals characteristic for the cobalt(II) porphyrins is associated with appearance of signals corresponding to mono-nitrene species of the type **3** (for an example, see Figure S5-1; Supporting Information). The room-temperature (r.t.) EPR measurement of the same samples gave spectra characteristic for ligand radical species (Figure 3, top),[42] and the simulated spectra fits best to a mono-nitrene species of the type **3**.

Scheme 3. Different Combinations of Cobalt(II) Porphyrins and Organic Azides Used to Study the Formation of Mono-Nitrene Species

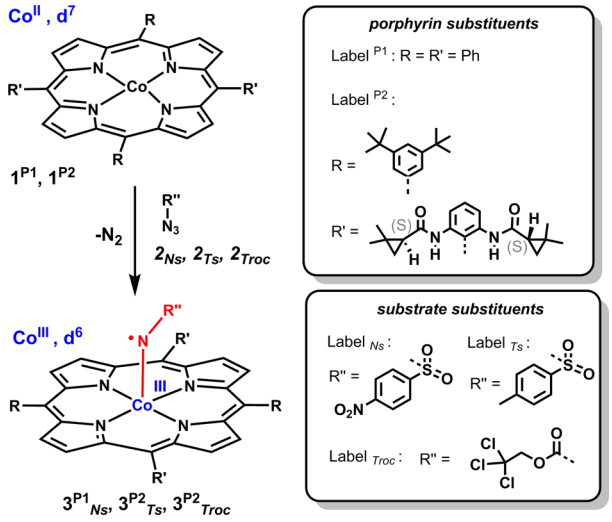

The X-band EPR spectrum recorded from a reaction mixture of $\mathbf{1}^{P1}$ and $\mathbf{2}_{Ns}$ in frozen benzene-d_6/*o*-terphenyl solution at 50 K was quite isotropic, but the *g*-anisotropy is clearly resolved in high-frequency (244 GHz) EPR measurements (Figure 3, bottom). The experimental *g*-anisotropy is very small, and smaller than calculated with DFT (Table 1). This may be caused by a small mismatch between the calculated and

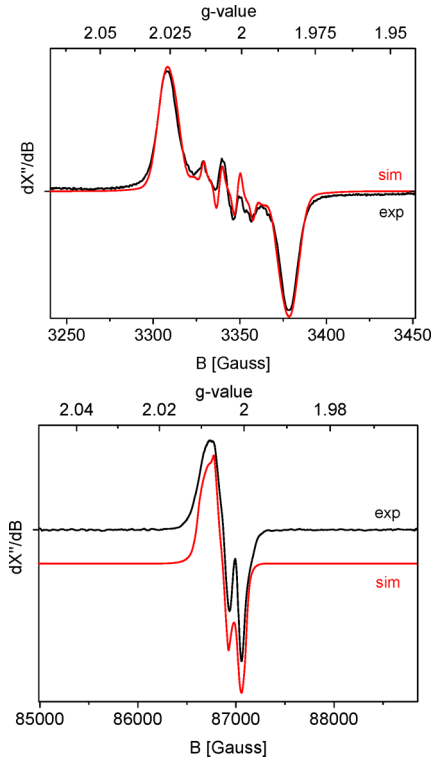

Figure 3. Top: Experimental and simulated (Table 1) X-band EPR spectra of nitrene radical ligand complex $\mathbf{3}^{P1}{}_{Ns}$ in solution at r.t. Isotropic spectrum in solution recorded at r.t.[42] (Freq = 9.38056 GHz; mod. amp. = 1 G; microwave power = 0.2 mW). Bottom: Experimental and simulated (Table 1) high-field EPR spectra of nitrene radical ligand complex $\mathbf{3}^{P1}{}_{Ns}$ obtained by mixing $\mathbf{1}^{P1}$ and $\mathbf{2}_{Ns}$ in frozen solution (Freq = 243.76176 GHz, mod. amp. = 1 mT, microwave power = 1 mW, *T* = 50 K).

experimental geometries, as the calculated **g**-tensor is sensitive to the orientation of the $-SO_2Ar$ fragment of the nitrene radical moiety (e.g., optimization with and without dispersion corrections). It should further be noted at this point that complexes of type $\mathbf{3}^{P1}{}_{Ns}$ need not be five-coordinate. Coordination of an additional ligand to the cobalt(III) center (see also Scheme S5-5; Supporting Information) is perhaps even likely (*vide infra*), and this will also have some influence on the (calculated) **g**-tensor and hyperfine coupling parameters of the mono-nitrene complex, albeit very small (see Table 1 for a comparison of the experimental EPR parameters and the DFT calculated values of five-coordinate $\mathbf{3}^{P1}{}_{Ns}$ and its six-coordinate $NsNH^-$ and OH^- adducts). Note that a variety of other six-coordinate analogs of $\mathbf{3}^{P1}{}_{Ns}$ investigated, containing either neutral or anionic ligands bound *trans* to the nitrene radical moiety, all have very similar calculated *g*-values and HFIs with cobalt and the nitrogen atom of the spin-bearing nitrene radical ligand (see Table S5-1, Supporting Information).

Additionally, a quite anisotropic cobalt hyperfine interaction (HFI) tensor was revealed by Q-band Davies ENDOR measurements. The Q-band Davies ENDOR experiment (Figure S5-2; Supporting Information) revealed broad features spanning 1−60 MHz. Apart from the characteristic proton signals centered around 52 MHz, strong lines are observed around 22 and 12 MHz. The position of these features is consistent with the ^{59}Co hyperfine parameters estimated from the high-field EPR spectrum (Figure 3), which are summarized in Table 1. Low-frequency contributions (<8 MHz) are

DOI: 10.1021/jacs.5b01197
J. Am. Chem. Soc. 2015, 137, 5468−5479

Table 1. EPR Parameters of Nitrene Radical Complex 3^{P1}_{Ns} in Frozen Solution at 50 K and in Isotropic Solution at Room Temperature

		50 K		298 K	
	g_{11}	g_{22}	g_{33}	g_{av}	g_{iso}
Exp	2.0087	2.0049	2.0005	2.0047	2.005
DFT [a]					
S-coord	*2.0490*	*2.0154*	*1.9810*	*2.0150*	*2.015*
S-coord[e]	*2.0287* [e]	*2.0029* [e]	*1.9816* [e]	*2.0044* [e]	*2.004* [e]
$NsNH^-$ [f]	*2.0311*	*2.0052*	*1.9966*	*2.0109*	*2.011*
OH^- [g]	*2.0387*	*2.0116*	*2.0022*	*2.0175*	*2.018*
A^{Co}	A^{Co}_{11} [b]	A^{Co}_{22} [b]	A^{Co}_{33} [b]	A^{Co}_{av} [b]	A^{Co}_{iso} [b]
Exp	–50 [c]	50 [c]	20 [c]	7 [c]	–25
DFT [a]					
S-coord	*-98*	*65*	*13*	*–7*	*–7*
S-coord[e]	*-18* [e]	*-89* [e]	*15* [e]	*-42* [e]	*-31* [e]
$NsNH^-$ [g]	*-59*	*30*	*11*	*-6*	*-6*
OH^- [h]	*-62*	*50*	*67*	*18*	*18*
A^{N}	A^{N}_{11} [b]	A^{N}_{22} [b]	A^{N}_{33} [b]	A^{N}_{av} [b]	A^{N}_{iso} [b]
Exp	n.r. [d]	n.r. [d]	n.r. [d]	n.r. [d]	10
DFT [a]					
S-coord	*–20*	*–14*	*81*	*15*	*16*
S-coord[e]	*–23* [e]	*–14* [e]	*84* [e]	*16* [e]	*16* [e]
$NsNH^-$ [f]	*–11*	*–9*	*87*	*22*	*22*
OH^- [g]	*–13*	*–10*	*84*	*20*	*20*

[a]Geometry of 3^{P1}_{Ns} optimized with Turbomole (full atom model, BP86, def2-TZVP) employing Grimme's D3-dispersion corrections (disp3); EPR parameters calculated with ORCA, (b3-lyp/def2-TZVP). [b]MHz. [c]Data from Q-band Davies ENDOR measurements (see Supporting Information). [d]Not resolved. [e]Geometry of 3^{P1}_{Ns} (full atom model) optimized with Turbomole at the b3-lyp, def2-TZVP level without dispersion corrections to match the solution data. [f]Optimized geometry of six-coordinate $NsNH^-$ amido adduct of 3^{P1}_{Ns} (full atom model, BP86, def2-TZVP) employing Grimme's D3-dispersion corrections (disp3). [g]Optimized geometry of six-coordinate OH^- hydroxido adduct of 3^{P1}_{Ns} (full atom model, BP86, def2-TZVP) employing Grimme's D3-dispersion corrections (disp3).

attributed to the porphyrin nitrogen atoms. The corresponding DFT calculated values match the experimental ones quite well (Table 1), albeit that the calculated anisotropy of the cobalt hyperfine tensor is a bit larger than in the experimental spectrum. Unfortunately, the anisotropic nitrene nitrogen hyperfine couplings were not resolved for technical reasons (see Supporting Information for discussion).

Interestingly, the mono-nitrene species **3** did not form instantaneously upon mixing the azides and the Co^{II}porphyrin catalysts at r.t. For example, only 10% of the mono-nitrene species 3^{P2}_{Troc} was formed upon mixing 1^{P2} and azide 2_{Troc} at r.t. after 15 min. These conversions were determined by comparison of the spin concentrations (double integration) with a sample of TEMPO of the same concentration. It should be mentioned that the relaxation times of TEMPO and the mono-nitrene species **3** are likely markedly different, and hence the spin integrations gave only a rough qualitative comparison of the spin concentrations. However, upon heating the samples, higher intensities were observed immediately; and on letting them heat overnight at 45 °C, the maximum intensities for all of these species were observed. The resulting solutions still contained the (excess) organic azide (as revealed by analysis of crystals recovered upon evaporation of the solvent) and were still catalytically active in aziridination of styrene (as confirmed by ^{1}H NMR and GC-MS analysis of the crude reaction mixture). Among the series of complexes and nitrene precursors studied, the maximum intensities were obtained for the combination of 1^{P2} and 2_{Troc} (see Figure 4). This can be

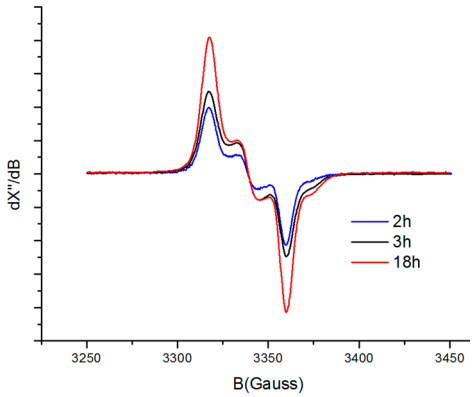

Figure 4. EPR spectra of 3^{P2}_{Troc} (r.t.; benzene-d_6) showing increasing intensities over time on heating at 45 °C.

explained on the basis of better stabilization of the formed nitrene radical intermediate by H-bonding between the amide arms of the porphyrin backbone in 1^{P2} and the nitrene transfer agent 2_{Troc}.[8,41] The concentration of this species was found to be ~80% referenced against a sample of TEMPO with the same concentration as the cobalt precursor. Similar rough spin counting reveals the presence of ~60% of EPR active 3^{P1}_{Ns} upon reaction of 1^{P1} with excess 2_{Ns} after heating overnight at 45 °C.

EPR Spectroscopy of the Bis-Nitrene Species 5^{P1}_{Ns}. In contrast to the use of organic azides that produced mono-nitrene species of the type **3** upon reaction with the cobalt(II) porphyrin complexes, reaction of an excess of *N*-nosyl iminoiodane 4_{Ns} with 1^{P1} at room temperature in benzene-d_6 yielded an entirely different species (Scheme 4), as revealed by

Scheme 4. Reaction of Cobalt(II) Porphyrin 1^{P1} and Nitrene Transfer Reagent 4_{Ns} To Give Bis-Nitrene Species 5^{P1}_{Ns} [a]

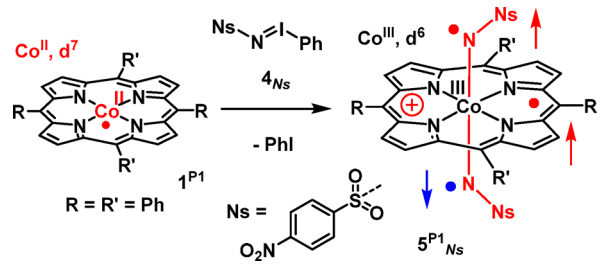

[a]Please note that the formation of a one-electron oxidized porphyrin ligand is indicated with a positive charge on the porphyrin ring, using the "π-cation radical" convention commonly used in cytochrome P450 chemistry,[74] but this is in fact a mono-anionic $por^{\bullet-}$ ligand.

X-band EPR spectroscopy in solution at r.t. A completely different isotropic spectrum was obtained with 4_{Ns} (Figure 5) than that with nosyl azide 2_{Ns} or tosyl azide 2_{Ts} (Figure 3, top). The multiline spectrum revealed an isotropic *g*-value close to g_e (2.003) with well-resolved hyperfine interactions with the two equivalent $N_{nitrene}$ atoms ($A^{N\text{-nitrene}}_{iso}$ = 10.0 MHz) and the four equivalent $N_{porphyrin}$ atoms ($A^{N\text{-por}}_{iso}$ = 3.5 MHz), again

DOI: 10.1021/jacs.5b01197
J. Am. Chem. Soc. 2015, 137, 5468–5479

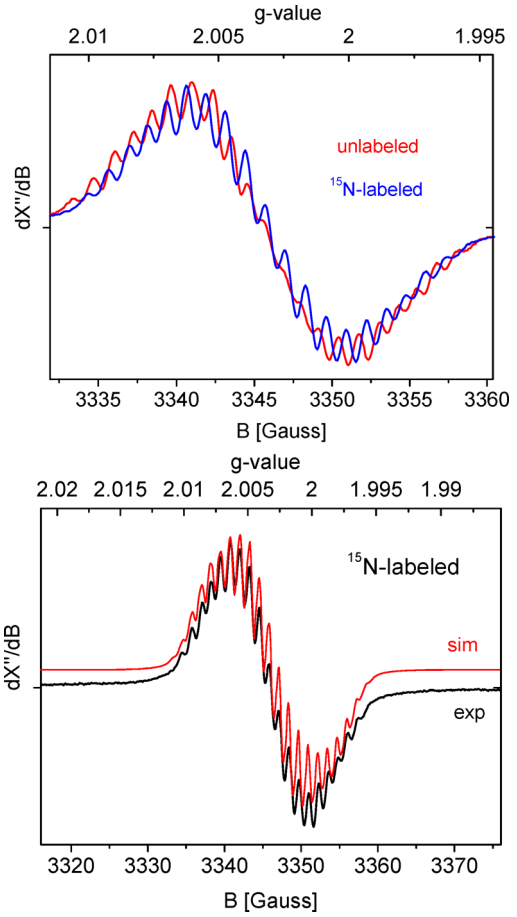

Figure 5. Top: Overlay of the isotropic X-band EPR spectra of unlabeled $\mathbf{5}^{\mathbf{P1}}{}_{\mathbf{Ns}}$ (red) and labeled $(^{15}\mathrm{N})_2$-$\mathbf{5}^{\mathbf{P1}}{}_{\mathbf{Ns}}$ (blue). Bottom: Experimental and simulated isotropic EPR spectra of species $(^{15}\mathrm{N})_2$-$\mathbf{5}^{\mathbf{P1}}{}_{\mathbf{Ns}}$ in benzene-d_6. Freq = 9.38126 GHz, mod. ampl. = 1 G, microwave power = 0.2 mW, T = 298 K.

indicating formation of a "ligand radical" complex. The isotropic cobalt HFI in $\mathbf{5}^{\mathbf{P1}}{}_{\mathbf{Ns}}$ ($A^{\mathrm{Co}}{}_{\mathrm{iso}}$ = 2.0 MHz) was very small, even smaller than in the mono-nitrene case (25 MHz). The spectrum could be satisfactorily simulated based on the DFT calculated EPR parameters (Figure 5 and Table 2).

To prove that the largest detected nitrogen hyperfine couplings stem from the two equivalent nitrene moieties, we further prepared the ^{15}N-labeled iminoiodane $^{15}\mathrm{N}$-$\mathbf{4}_{\mathbf{Ns}}$ (PhI=^{15}NNs) and recorded the r.t. EPR spectrum of $(^{15}\mathrm{N})_2$-$\mathbf{5}^{\mathbf{P1}}{}_{\mathbf{Ns}}$ generated in a mixture of $\mathbf{1}^{\mathbf{P1}}$ and $^{15}\mathrm{N}$-$\mathbf{4}_{\mathbf{Ns}}$. This led to clear differences in the hyperfine coupling pattern compared to the non-labeled analogue $\mathbf{5}^{\mathbf{P1}}{}_{\mathbf{Ns}}$ (Figure 5, top).

Table 2. Experimental (298 K)[a] and DFT[b] Calculated EPR Parameters of $\mathbf{5}^{\mathbf{P1}}{}_{\mathbf{Ns}}$ and $(^{15}\mathrm{N})_2$-$\mathbf{5}^{\mathbf{P1}}{}_{\mathbf{Ns}}$

	Equiv. Nuclei	Exp [a)]	*DFT* [b)]
g_{iso}		2.003	*2.008*
$A^{\mathrm{Co}}{}_{iso}$ [c)]	1 (I = 7/2)	−2.0	*−2.5*
$A^{\text{N-nitrene}}{}_{iso}$ ^{14}N [c)]	2 (I = 1)	10.0	*16.0* [d)]
$A^{\text{N-nitrene}}{}_{iso}$ ^{15}N [c)]	2 (I = ½)	14.0	*22.4*
$A^{\text{N-por}}{}_{iso}$ [c)]	4 (I = 1)	3.5	*−1.5* [e)]

[a]Derived from spectral simulations shown in Figure 5. [b]Geometry optimized with Turbomole (b3-lyp/def2-TZVP) using a simplified model of $\mathbf{5}^{\mathbf{P1}}{}_{\mathbf{Ns}}$ without porphyrin Ph substituents without dispersion corrections to match the r.t. solution EPR data. EPR parameters calculated with ORCA (b3-lyp/def2-TZVP). [c]MHz. [d]Average of two $A^{\text{N-nitrene}}$ hyperfines. [e]Average of four $A^{\text{N-por}}$ hyperfines.

EPR simulation using an expected 1.4 times larger $A^{\text{N-nitrene}}{}_{\mathrm{iso}}$ ^{15}N (I = 1/2) hyperfine coupling (14 MHz) compared to the unlabeled ^{14}N $A^{\text{N-nitrene}}{}_{\mathrm{iso}}$ constant of 10 MHz (I = 1) in $\mathbf{5}^{\mathbf{P1}}{}_{\mathbf{Ns}}$ and otherwise identical spectral parameters provided an excellent fit of the experimental spectrum (Figure 5, bottom; Table 2). Hence, the largest detected nitrogen hyperfine couplings indeed stem from the two equivalent nitrene moieties.

In case of the bis-nitrene species $\mathbf{5}^{\mathbf{P1}}{}_{\mathbf{Ns}}$ the intensity of the signal was not as strong as the mono-nitrene species, for example, $\mathbf{3}^{\mathbf{P1}}{}_{\mathbf{Ns}}$. On heating the sample shortly, the intensity increased only very slightly and was at least 10 times lower than that of the mono-nitrene species (spin counting amounts to ∼8%, using a reference sample containing TEMPO at the same concentration as $\mathbf{1}^{\mathbf{P1}}$). The poor solubility of the *N*-nosyl iminoiodane substrate in benzene-d_6 could well be a reason for the low intensities obtained for species $\mathbf{5}^{\mathbf{P1}}{}_{\mathbf{Ns}}$. It is also worth mentioning that the experimentally detected signal of species $\mathbf{5}^{\mathbf{P1}}{}_{\mathbf{Ns}}$ stems from a (net) doublet spin state (S = 1/2), leading to the characteristic EPR data shown in Figure 5 and Table 2, but in DFT (b3-lyp) the doublet (S = 1/2) and quartet (S = 3/2; ΔG = +0.2 kcal mol^{-1}) spin states of $\mathbf{5}^{\mathbf{P1}}{}_{\mathbf{Ns}}$ are predicted to be of nearly equal energy.[75] As only the doublet state is detectable with EPR at r.t. in solution, the potential existence of a (slow) thermal equilibrium between the two spin states might also explain the relatively low EPR intensity of the signal, which stems from the S = 1/2 state of bis-nitrene species only. Furthermore, a word about the higher reactivity (intrinsic instability) of these bis-nitrene species is worth mentioning. In contrast to the mono-nitrene species $\mathbf{3}^{\mathbf{P1}}{}_{\mathbf{Ns}}$, which increased in time upon heating the solution to 45 °C, species $\mathbf{5}^{\mathbf{P1}}{}_{\mathbf{Ns}}$ decomposed at this temperature, causing the EPR signal of the bis-nitrene species to disappear completely overnight (i.e., in absence of other substrates). Catalyst decomposition may be less important in the presence of suitable substrates, as heating the solution in the presence of styrene did reveal the expected aziridination activity (as confirmed by ^{1}H NMR and GC-MS analysis of the crude reaction mixture).

Steric and Electronic Influence of the Catalyst on Formation of the Nitrene Intermediates. The steric and electronic influence of the catalyst on the species obtained, even when using the more oxidizing *N*-nosyl iminoiodane $\mathbf{4}_{\mathbf{Ns}}$, is quite dramatic. For example, on using the bulkier porphyrin complex $\mathbf{1}^{\mathbf{P2}}$ in combination with the oxidizing *N*-nosyl iminoiodane $\mathbf{4}_{\mathbf{Ns}}$, the bis-nitrene species was detected only in minor amounts. Instead, a major EPR signal corresponding to the mono-nitrene species was detected. Thus, it may be concluded that the bulky side groups on the porphyrin backbone of $\mathbf{1}^{\mathbf{P2}}$ make it difficult for the second molecule of *N*-nosyl iminoiodane $\mathbf{4}_{\mathbf{Ns}}$ to react.

In contrast to the decomposition observed for species $\mathbf{5}^{\mathbf{P1}}{}_{\mathbf{Ns}}$ that was obtained from a mixture of $\mathbf{1}^{\mathbf{P1}}$ and an excess of $\mathbf{4}_{\mathbf{Ns}}$, mono-nitrene species $\mathbf{3}^{\mathbf{P2}}{}_{\mathbf{Ns}}$ obtained from a mixture of $\mathbf{1}^{\mathbf{P2}}$ and excess $\mathbf{4}_{\mathbf{Ns}}$ proved to be much more stable. On heating the latter sample to 45 °C, the signal intensity decreased, with the complete disappearance of the initially detected small amount of bis-nitrene species $\mathbf{5}^{\mathbf{P2}}{}_{\mathbf{Ns}}$. However, a significant amount of mono-nitrene species $\mathbf{5}^{\mathbf{P2}}{}_{\mathbf{Ns}}$ remained present in solution, even after heating for a period of 18 h (Figure 6). This was also

DOI: 10.1021/jacs.5b01197
J. Am. Chem. Soc. 2015, 137, 5468−5479

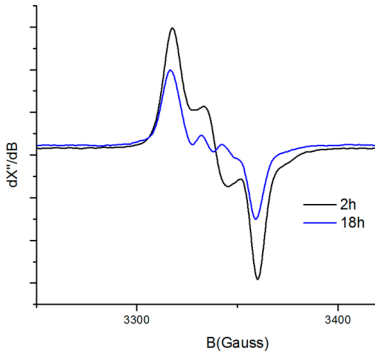

Figure 6. EPR spectra of $\mathbf{1}^{P2}$ with $\mathbf{4}_{Ns}$. Sample obtained by heating the reaction mixture to 45 °C; spectra recorded at r.t. in benzene-d_6. Note the decrease in the intensity of the signal over time.

observed with ESI-MS measurements (Figure S4-20; Supporting Information). These results clearly show that the bis-nitrene species **5** is more reactive than the mono-nitrene species **3** and that complex $\mathbf{1}^{P2}$ is more stable than complex $\mathbf{1}^{P1}$ when combined with *N*-nosyl iminoiodane $\mathbf{4}_{Ns}$. The latter can perhaps be attributed to stabilizing H-bonding interactions between the nitrene radical moiety and the H-bond-donating amido functionalities incorporated in the porphyrin backbone of $\mathbf{1}^{P2}$, as was previously observed in aziridination reactions and studied previously using DFT.[8,41] At the same time, it also suggests that *N*-nosyl iminoiodane $\mathbf{4}_{Ns}$ is not a very benign nitrene transfer reagent for these reactions as it seems to undergoes subsequent side reactions with the catalyst (especially for the less bulky catalysts and in the absence of another substrate).

UHR-ESI-MS Spectrometry. To further corroborate the above observations in the EPR measurements, the reactions were also investigated with mass spectrometry. We investigated the formation of both the mono- and the bis-nitrene species. High-resolution ESI-MS mass spectrometry proved to be a suitable method to detect the formation of both mono- and bis-nitrene species. However, since these species are neutral (or perhaps anionic, *vide infra*), only signals resulting from protonation, (one-electron) oxidation, and formation of Na^+ adducts can be expected in positive mode UHR-ESI-MS.

A reaction mixture of $\mathbf{1}^{P1}$ with nosyl azide $\mathbf{2}_{Ns}$ in C_6D_6/MeCN produced clear ESI-MS signals around m/z 872 characteristic for formation of the mono-nitrene species $\mathbf{3}^{P1}{}_{Ns}$ (Scheme 3). The isotope distribution pattern and exact masses determined by ESI-MS match the theoretical values ($\Delta m/z$ < 0.004 Da) for the species in its protonated form $[\mathbf{3}^{P1}{}_{Ns} + H]^+$ (Figure 7a). The relatively low intensity of the detected nitrene

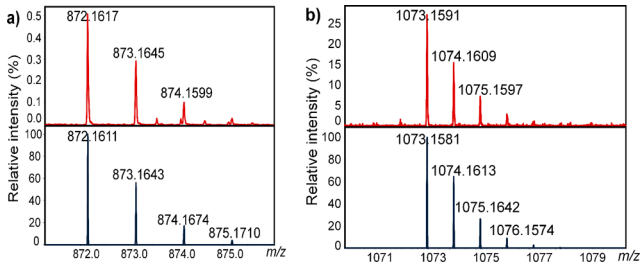

Figure 7. Observed (top) and simulated (bottom) ESI-MS spectrum with isotope distribution (a) $[\mathbf{3}^{P1}{}_{Ns} + H^+]$ (870−876 au) and (b) $[\mathbf{5}^{P1}{}_{Ns} + H^\bullet + H^+]$ (1070−1080 au).

radical species derived from reaction of complex $\mathbf{1}^{P1}$ with azide $\mathbf{2}_{Ns}$ is likely a result of incomplete conversion to $\mathbf{3}^{P1}{}_{Ns}$, as the measurements were performed within 30 min of sample preparation. At the same time, subsequent reactions with the cosolvent acetonitrile cannot be neglected. While $\mathbf{3}^{P1}{}_{Ns}$ is detected as a five-coordinate species in its protonated form with ESI-MS, this does not exclude $\mathbf{3}^{P1}{}_{Ns}$ from being six-coordinate (see Scheme S5-5; Supporting Information), as the sixth ligand might easily dissociate in the ionization chamber of the ESI-MS spectrometer. We were not able to detect $\mathbf{3}^{P1}{}_{Ns}$ in negative mode ESI-MS measurements (cold-spray ionization). However, interestingly, in the positive mode ESI-MS measurements (cold-spray ionization), a Na^+ adduct of NO_2PhSO_2NHD was detected from a mixture of $\mathbf{1}^{P1}$ and $\mathbf{2}_{Ns}$. Note that formation of $NO_2PhSO_2ND^\bullet$ radicals, detected with EPR, has been reported earlier.[8] On this basis, the most likely candidates for the sixth ligand coordinated to the mono-nitrene species are either the NO_2PhSO_2NDH amine ligand or the $NO_2PhSO_2ND^-$ amido ligand (in both cases detected as the Na^+ adduct of the amine in the ESI-MS measurements, in the first case directly and in the second case after HAT).

ESI-MS spectra recorded from a mixture of $\mathbf{1}^{P1}$ and *N*-nosyl iminoiodane $\mathbf{4}_{Ns}$ revealed signals pointing to the presence of bis-nitrene species $\mathbf{5}^{P1}{}_{Ns}$ (Scheme 4). This species was observed as the protonated form of its hydrogen atom abstraction (HAA) reaction product ($[\mathbf{5}^{P1}{}_{Ns} + H^\bullet + H^+]$), thus pointing to rapid HAA from the cosolvent MeCN (Figure 7b). Substantially weaker signals corresponding to the mono-nitrene species $\mathbf{3}^{P1}{}_{Ns}$ were still detected ($[\mathbf{3}^{P1}{}_{Ns} + H]^+$), which likely resulted from incomplete conversion of $\mathbf{1}^{P1}$ to $\mathbf{5}^{P1}{}_{Ns}$ and/or fragmentation of $\mathbf{5}^{P1}{}_{Ns}$ to $\mathbf{3}^{P1}{}_{Ns}$ in the ionization chamber of the ESI-MS spectrometer.

Electronic Structures and UV−vis Spectra of Mono- and Bis-Nitrene Species. To gain additional insight into the electronic structures of the generated nitrene species, we performed DFT geometry optimizations at the b3-lyp/def2-TZVP level using the simplified models $\mathbf{3}^{P0}{}_{Ns}$ and $\mathbf{5}^{P0}{}_{Ns}$ without *meso*-phenyl substituents on the porphyrin ring P^0 (Figure 8). According to these calculations, mono-nitrene species $\mathbf{3}^{P1}{}_{Ns}$ formed from $\mathbf{1}^{P1}$ and $\mathbf{2}_{Ns}$ is best described as a Co^{III} species with one 1e reduced nitrene moiety and a normal, non-oxidized (por^{2-}) porphyrin ligand. Note again the experimental complex $\mathbf{3}^{P1}{}_{Ns}$ needs not be five-coordinate. Coordination of an

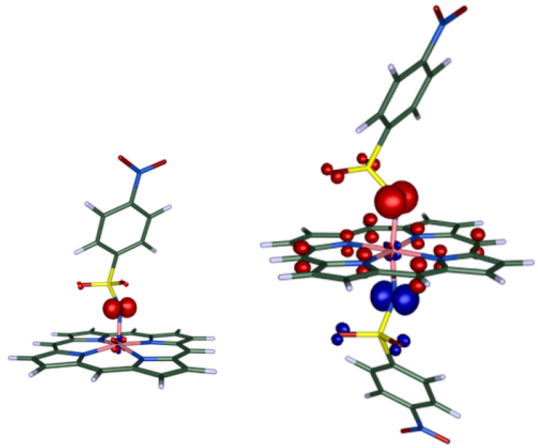

Figure 8. Spin density plots (b3-lyp/def2-TZVP) of mono-nitrene species $\mathbf{3}^{P0}{}_{Ns}$ (left) and bis-nitrene species $\mathbf{5}^{P0}{}_{Ns}$ (right).

DOI: 10.1021/jacs.5b01197
J. Am. Chem. Soc. 2015, 137, 5468−5479

additional ligand to the cobalt(III) center cannot be excluded (Scheme S5-5; Supporting Information) and even seems likely (*vide infra*). However, note that all six-coordinate analogs of $\mathbf{3}^{\mathbf{P0}}{}_{\mathbf{Ns}}$ considered computationally have almost identical spin density distributions as the one shown for five-coordinate mono-nitrene complex $\mathbf{3}^{\mathbf{P0}}{}_{\mathbf{Ns}}$ in Figure 8. In these calculations full atom models were optimized at the BP86/def2-TZVP/disp3 level (Turbomole), followed by single point calculations at the b3-lyp/def2-TZVP level (ORCA), considering several different (neutral and anionic) ligands bound *trans* to the nitrene radical moiety (see also Table S5-1; Supporting Information).

The bis-nitrene species $\mathbf{5}^{\mathbf{P0}}{}_{\mathbf{Ns}}$, on the other hand, is a triple-radical containing two 1e-reduced nitrene-moieties and a 1e-oxidized porphyrin ring (from por^{2-} to the $por^{\bullet-}$ radical monoanion). As is clear from the positive and negative spin density distribution (Figure 8, right), two of the three unpaired electrons in $\mathbf{5}^{\mathbf{P0}}{}_{\mathbf{Ns}}$ are antiferromagnetically coupled, thus effectively leading to a (net) doublet state ($S_{total} = 1/2$). Both $\mathbf{3}^{\mathbf{P1}}{}_{\mathbf{Ns}}$ and $\mathbf{5}^{\mathbf{P0}}{}_{\mathbf{Ns}}$ were found to contain a low-spin d^6 ($S_{Co} = 0$) Co^{III} center. Hence, formation of **5** involves one-electron oxidation of Co^{II} to Co^{III} upon formation of the first nitrene-radical (**3**) and a second intramolecular electron transfer from the porphyrin ring to the second nitrene moiety in the second step.

The DFT calculated electronic structures are qualitatively in agreement with UV−vis measurements, revealing the presence of a non-oxidized porphyrin ring in $\mathbf{3}^{\mathbf{P1}}{}_{\mathbf{Ns}}$ and a "porphyrin radical" ligand in $\mathbf{5}^{\mathbf{P1}}{}_{\mathbf{Ns}}$ (Figures 9 and 10).

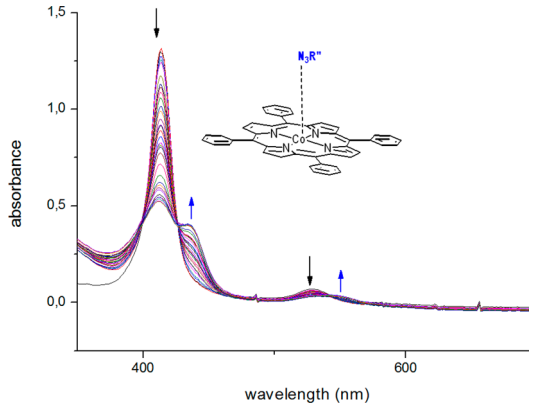

Figure 9. UV−vis spectra of a mixture of $\mathbf{1}^{\mathbf{P1}}$ and $\mathbf{2}_{\mathbf{Ns}}$ followed in time (after 40 min of sample preparation). Clear shifts in both the Q- and Soret-bands were observed corresponding to azide ligation to the cobalt(II) center.

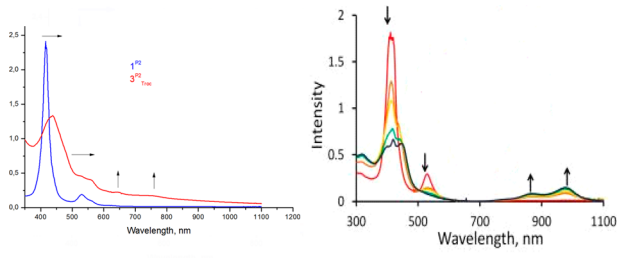

Figure 10. UV−vis spectral changes upon reaction of (left) complex $\mathbf{1}^{\mathbf{P2}}$ with azide $\mathbf{2}_{\mathbf{Troc}}$ to give mono-nitrene species $\mathbf{3}^{\mathbf{P2}}{}_{\mathbf{Troc}}$ formed after heating the solution overnight, and (right) reaction of complex $\mathbf{1}^{\mathbf{P1}}$ with iminoiodane $\mathbf{4}_{\mathbf{Ns}}$ to give bis-nitrene species $\mathbf{5}^{\mathbf{P1}}{}_{\mathbf{Ns}}$ within 1 h.

Metal- (not porphyrin-) centered oxidation of Co^{II}(por) to Co^{III}(por) is known to produce characteristic red-shifts of both the Soret- and Q-bands.[76,77] The same is also true for binding donor ligands, such as pyridine or bipyridyl ligands, to the central metal ion of cobalt(II) porphyrins.[78,79] Such shifts were indeed observed upon measuring UV−vis spectra of a mixture of $\mathbf{1}^{\mathbf{P1}}$ and $\mathbf{2}_{\mathbf{Ns}}$ immediately upon mixing. In Figure 9, the UV−vis spectrum of a mixture of $\mathbf{1}^{\mathbf{P1}}$ and $\mathbf{2}_{\mathbf{Ns}}$ was followed in time (after 40 min of sample preparation). In these spectra, the observed shifts in the Q- and Soret-bands are due to formation of a simple azide adduct (mostly likely a monoazide adduct). Indeed, measuring EPR spectra of these same mixtures (again 40 min after mixing the reagents) without any additional heating revealed extremely weak EPR signals in the region around $g = 2.0$, corresponding to formation of only a tiny amount of nitrene radical species $\mathbf{3}^{\mathbf{P1}}{}_{\mathbf{Ns}}$.

On measuring the UV−vis spectra of these same solutions after heating them overnight at 45 °C (i.e., solutions that gave strong EPR signals characteristic for $\mathbf{3}^{\mathbf{P1}}{}_{\mathbf{Ns}}$) clearly revealed the presence of a new species in the UV−vis spectra (Figure S6-2, Supporting Information), concomitant with much higher EPR intensities corresponding to nitrene radical species $\mathbf{3}^{\mathbf{P1}}{}_{\mathbf{Ns}}$. Illustrative spectra comparing $\mathbf{1}^{\mathbf{P2}}$ and species $\mathbf{3}^{\mathbf{P2}}{}_{\mathbf{Troc}}$ formed upon heating a solution of complex $\mathbf{1}^{\mathbf{P2}}$ in the presence of an excess of $\mathbf{2}_{\mathbf{Troc}}$ are shown in Figure 10 (left).

Reaction of complex $\mathbf{1}^{\mathbf{P2}}$ with azide $\mathbf{2}_{\mathbf{Troc}}$ resulted in red-shifts of the Soret band at 438 nm and shifting of the Q-band to 648 nm. In addition, a new peak at ∼753 nm was also observed (Figure 10, left). The shift in the Soret and the Q-band is indicative of oxidation of the metal from cobalt(II) to cobalt(III) and (or) ligation to the sixth coordination site, leaving the porphyrin ligand intact without oxidation upon formation of mono-nitrene radical species $\mathbf{3}^{\mathbf{P2}}{}_{\mathbf{Troc}}$. The additional band at ∼753 nm is likely a charge-transfer band (e.g., a MLCT or LMCT band involving the nitrene radical and the cobalt(III) center).

Formation of porphyrin-based ligand radicals is known to cause drastic changes in the UV−vis spectrum with appearance of red-shifted bands, disappearance of the Q-band and obvious shape changes of the Soret band compared to unmodified (i.e., non-reduced/nonoxidized) dianionic porphyrinato ligands (por^{2-}).[80,81] This is what was observed upon formation of bis-nitrene species $\mathbf{5}^{\mathbf{P1}}{}_{\mathbf{Ns}}$ in the reaction of complex $\mathbf{1}^{\mathbf{P1}}$ with *N*-nosyl iminoiodane $\mathbf{4}_{\mathbf{Ns}}$ (Figure 10, right). As mentioned before, when using iminoiodane $\mathbf{4}_{\mathbf{Ns}}$, formation of the bis-nitrene species is comparatively faster than formation of the mono-nitrenes when using azide $\mathbf{2}_{\mathbf{Ns}}$. Accordingly, in the case on measuring the UV−vis spectra of a mixture of $\mathbf{1}^{\mathbf{P1}}$ and $\mathbf{4}_{\mathbf{Ns}}$, the disappearance and shape changes of the Q- and Soret-bands was observed within an hour of making these samples (Figure 10, right). As shown in Figure 10, the species exhibited characteristic, strongly red-shifted bands at 863 and 977 nm. Similar spectral changes have been reported for Co^{III} complexes with a 1e-oxidized octaethylporphyrin ligand.[82,83] Hence, we assign these spectral changes to formation of the bis-nitrene species $\mathbf{5}^{\mathbf{P1}}{}_{\mathbf{Ns}}$. This is also in correspondence with the EPR measurements. Both the EPR and UV−vis signals characteristic for the nitrene radical species $\mathbf{5}^{\mathbf{P1}}{}_{\mathbf{Ns}}$ were completely lost upon heating the mixture overnight at 45 °C.

In accordance with the EPR spectroscopic studies, once again the mono-nitrene species $\mathbf{3}^{\mathbf{P2}}{}_{\mathbf{Troc}}$ was found to be more stable than bis-nitrene species $\mathbf{5}^{\mathbf{P1}}{}_{\mathbf{Ns}}$. UV−vis spectroscopy clearly indicated that solutions of $\mathbf{3}^{\mathbf{P2}}{}_{\mathbf{Troc}}$ obtained from complex $\mathbf{1}^{\mathbf{P2}}$

DOI: 10.1021/jacs.5b01197
J. Am. Chem. Soc. 2015, 137, 5468−5479

and $\mathbf{4}_{\mathrm{Troc}}$ remained stable for even 2 days, while a significant amount of decomposition already occurred for $\mathbf{5}^{\mathbf{P1}}{}_{\mathbf{Ns}}$ obtained from complex $\mathbf{1}^{\mathbf{P1}}$ and $\mathbf{4}_{\mathbf{Ns}}$ within 2 h. This points to a higher intrinsic reactivity of bis-nitrene species $\mathbf{5}^{\mathbf{P1}}{}_{\mathbf{Ns}}$ compared to mono-nitrene species $\mathbf{3}^{\mathbf{P1}}{}_{\mathbf{Ns}}$. Indeed, DFT calculations (using **3′** and **5′**, which are simplified models of $\mathbf{3}^{\mathbf{P1}}{}_{\mathbf{Ns}}$ and $\mathbf{5}^{\mathbf{P1}}{}_{\mathbf{Ns}}$ without phenyl substituents on the porphyrin ring and having a *N*-SO_2Ph base nitrene instead of *N*-Ns) predict a ca. 1.3 kcal mol^{-1} lower activation energy for HAA from ethylbenzene for **5′** ($\Delta G^{\ddagger}$ = +30.4 kcal mol^{-1}) than for **3′** ($\Delta G^{\ddagger}$ = +31.7 kcal mol^{-1}).

X-ray Absorption Spectroscopic (XAS) Studies. To gain additional evidence for the coordination mode and the oxidation states of the two intermediates, i.e., the mono- and the bis-nitrene species, XAS measurements were performed. X-ray absorption near edge spectroscopic (XANES) studies were carried out at Co K-edge in order to directly probe the metal oxidation states in $\mathbf{3}^{\mathbf{P1}}{}_{\mathbf{Ns}}$, $\mathbf{3}^{\mathbf{P2}}{}_{\mathbf{Troc}}$, and $\mathbf{5}^{\mathbf{P1}}{}_{\mathbf{Ns}}$ (Figure 11A). The

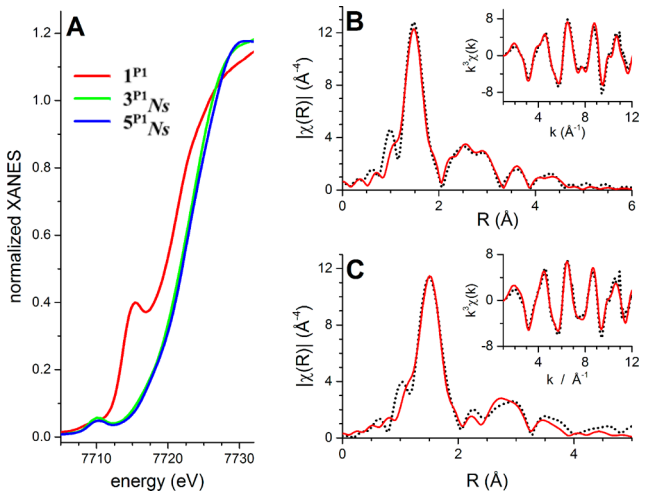

Figure 11. (A) XANES of $\mathbf{1}^{\mathbf{P1}}$ (red), $\mathbf{3}^{\mathbf{P1}}{}_{\mathbf{Ns}}$ (green), and $\mathbf{5}^{\mathbf{P1}}{}_{\mathbf{Ns}}$ (blue). Spectra are referenced to the first inflection point of a cobalt reference foil set to 7709.0 eV. (B) Fourier transform EXAFS spectra of $\mathbf{5}^{\mathbf{P1}}{}_{\mathbf{Ns}}$ (dotted line) and the best fit (red line); the inset shows the EXAFS data on a wave vector scale weighted by k^3 with respective representation. (C) Fourier transform EXAFS spectra of $\mathbf{3}^{\mathbf{P1}}{}_{\mathbf{Ns}}$ (dotted line) and the best fit (red line); the inset shows the EXAFS data on a wave vector scale weighted by k^3 with respective representation. For further details see Supporting Infomation.

starting cobalt(II)-*meso*-tetraphenylporphyrin (TPP) complex $\mathbf{1}^{\mathbf{P1}}$ exhibited an edge inflection energy of ca. 7720.7 eV. A shoulder feature along the rising edge at 7715.4 eV corresponds to a 1s to 4p + LMCT shakedown transition, in accord with the observed four-coordinate square-planar structure of this complex. This transition is strongest in four-coordinate square-planar Co complexes, but is also observed in five-coordinate square-pyramidal geometries (it is not present in either T_d or O_h geometries). Finally, a broad 1s to 3d pre-edge peak was observed at 7708.9 eV, with preliminary peak fitting analysis indicating a peak area of approximately 8.1 units. The energies of the edge and 1s → 3d pre-edge transitions are in accord with the reported values for other cobalt(II) complexes.[80,81] XANES of $\mathbf{5}^{\mathbf{P1}}{}_{\mathbf{Ns}}$ showed a +1.9 eV blue-shift of the edge inflection energy to 7722.56 eV, relative to complex $\mathbf{1}^{\mathbf{P1}}$, supporting metal-centered oxidation from cobalt(II) to cobalt(III). The 1s → 3d pre-edge transition was also blue-shifted by ∼1.0 to 7710.2 eV and the pre-edge increased in intensity (peak-area of 12.0 units). Most notably, $\mathbf{5}^{\mathbf{P1}}{}_{\mathbf{Ns}}$ lacks the diagnostic 1s → 4p shakedown transition shoulder on the rising edge, providing strong evidence for a six-coordinate O_h cobalt site. Finally, the XANES data on $\mathbf{3}^{\mathbf{P1}}{}_{\mathbf{Ns}}$ revealed the existence of edge and 1s → 3d pre-edge transitions at nearly identical positions (7722.8 and 7710.2 eV, respectively) relative to $\mathbf{5}^{\mathbf{P1}}{}_{\mathbf{Ns}}$, thereby indicating that both mono-nitrene complex $\mathbf{3}^{\mathbf{P1}}{}_{\mathbf{Ns}}$ and bis-nitrene complex $\mathbf{5}^{\mathbf{P1}}{}_{\mathbf{Ns}}$ are cobalt(III) species.

Importantly, similar to the observations for complex $\mathbf{5}^{\mathbf{P1}}{}_{\mathbf{Ns}}$, the absence of the 1s → 4p shakedown transition in the XAS data of $\mathbf{3}^{\mathbf{P1}}{}_{\mathbf{Ns}}$ also points to the presence of a six-coordinate O_h cobalt(III) center for this complex. XANES data were also obtained for complex $\mathbf{3}^{\mathbf{P2}}{}_{\mathbf{Troc}}$ and compared with that for $\mathbf{3}^{\mathbf{P1}}{}_{\mathbf{Ns}}$ and $\mathbf{5}^{\mathbf{P1}}{}_{\mathbf{Ns}}$. Careful examination of the pre-edge of the XANES of different catalyst and oxidant combinations shows no distinct differences between the different generated intermediates (see Figure S3-1; Supporting Information). This indicates that six-coordinate O_h species were formed in all cases. Extended X-ray absorption fine structure (EXAFS) analysis revealed further structural details (Figures 11B–C and S3-2, S3-3 and Tables 3, S3-1, S3-2, and S3-3). For complex $\mathbf{5}^{\mathbf{P1}}{}_{\mathbf{Ns}}$, the first coordination sphere could be satisfactorily fitted by considering six N/O scatterers at a distance of 1.92 Å (Table 3). Although the additional outer-shell features could be satisfactorily accounted for by considering single scattering paths involving 8 carbons at 2.94 Å, 12 carbons at 3.35 Å, and 4 oxygen donors at 3.57 Å distance from cobalt, the fit could be significantly improved by introducing multiple-scattering pathways. The best fit for $\mathbf{5}^{\mathbf{P1}}{}_{\mathbf{Ns}}$ is represented by fit 12 in Table S3-1 and Figure 11B. It is important to note that efforts were also made to include the effect of the sulfur scatterers originating from the two −NNs units. However, all fits (fits 9–11 in Table S3-1) including any kind of S-shell showed negative Debye–Waller factors in the fit parameters; and hence they were not considered in the fitting procedure.

Interestingly, consistent with the XANES data, our attempts to do a set of fits for a back transformation range limited to the first shell (r = 0.8 − 2.1 Å) for $\mathbf{3}^{\mathbf{P1}}{}_{\mathbf{Ns}}$ also pointed to a six-

Table 3. A Comparison of the EXAFS Determined Metrical Parameters (for the first three shells) of $\mathbf{3}^{\mathbf{P1}}{}_{\mathbf{Ns}}$ and $\mathbf{5}^{\mathbf{P1}}{}_{\mathbf{Ns}}$ with That of the DFT Calculated Values for $\mathbf{3}^{\mathbf{P1}}{}_{\mathbf{Ns}}$(Ns-NH$^-$) and $\mathbf{5}^{\mathbf{P1}}{}_{\mathbf{Ns}}$[a]

	Co−N/C			Co···C/N			Co···C/N		
complex	n	r	σ^2	n	r	σ^2	n	r	σ^2
$\mathbf{3}^{\mathbf{P1}}{}_{\mathbf{Ns}}$ (EXAFS)	6	1.95	3.7	8	2.99	6.6	12	3.39	14.5
$\mathbf{3}^{\mathbf{P1}}{}_{\mathbf{Ns}}$(Ns-NH$^-$) (DFT)	6	1.94		8	2.98		12	3.92	
$\mathbf{5}^{\mathbf{P1}}{}_{\mathbf{Ns}}$ (EXAFS)	6	1.92	3.0	8	2.94	4.5	12	3.35	8.7
$\mathbf{5}^{\mathbf{P1}}{}_{\mathbf{Ns}}$ (DFT)	6	1.92		8	2.97		12	3.91	

[a]Details of the EXAFS simulation and DFT structures can be found in the Supporting Information.

DOI: 10.1021/jacs.5b01197
J. Am. Chem. Soc. 2015, 137, 5468–5479

coordinate geometry (fits 1−3; Table S3-2). This contrasts with previous assumptions considering mono-nitrene species $3^{P1}{}_{Ns}$ to be five-coordinate.[8,42] The best fit to the data of the mono-nitrene species requires six N/O scatterers at ∼1.95 Å distance from the cobalt(III) center, which is slightly longer (although almost identical within the error of measurements) than the Co−N distance of 1.92 Å obtained from the EXAFS data of bis-nitrene species $5^{P1}{}_{Ns}$.

With these results in hand, we set out to consider plausible ligands that could occupy the sixth coordination site for the mono-nitrene species $3^{P1}{}_{Ns}$. Initially, we considered coordination of a neutral unreacted nosyl azide ligand under the conditions of the EXAFS measurements. However, DFT geometry optimizations and calculation of the Co K-edge features of the optimized structures with DFT methods revealed that such nosyl azide species have too long Co−N distances to explain the experimental XAS data (Figures S8-2; Supporting Information). The same holds for the aqua adduct of $3^{P1}{}_{Ns}$. The Ns-NH_2 amine and ammonia (NH_3) adducts of $3^{P1}{}_{Ns}$ have shorter Co−N bond distances, which substantially decreases the calculated intensity of the pre-edge transitions in the Co K-edge region. However, the best agreement between the calculated and experimental pre-edge intensities is obtained for anionic ligand adducts of mono-nitrene $3^{P1}{}_{Ns}$. The optimized geometries of $NsNH^-$, NH_2^-, and OH^- adducts of $3^{P1}{}_{Ns}$ species have comparable Co−N and Co−X distances for the nitrene radical ligand and the sixth ligand X (Figure 12),

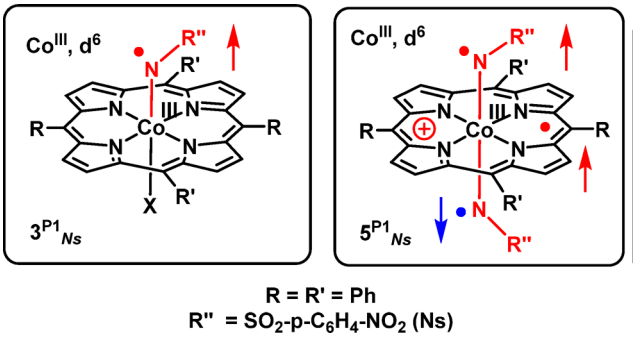

Figure 12. Left: The six-coordinate mono-nitrene species of the type $3^{P1}{}_{Ns}$ obtained from 1^{P1} and organic azide 2_{Ns}. Right: The six-coordinate bis-nitrene species $5^{P1}{}_{Ns}$ obtained from 1^{P1} and *N*-nosyl-iminoiodane 4_{Ns}.

respectively. Hence, similar pre-edge intensities are also computed as obtained for bis-nitrene species $5^{P1}{}_{Ns}$ (Figure S8-3; Supporting Information). Considering the detection of the Na^+ adduct of NO_2PhSO_2NHD as mentioned earlier in the ESI-MS studies in combination with the above-mentioned calculated pre-edge intensities, the $NsNH^-$ amido ligand is perhaps the most probable candidate occupying the sixth coordination site of the mono-nitrene species. Notably, the DFT calculated geometrical parameters for $3^{P1}{}_{Ns}(NsNH^-)$ is in reasonable agreement with the EXAFS data (Table 3). This would mean, however, that $3^{P1}{}_{Ns}$ is anionic (perhaps containing an $NsNH_3^+$ counterion). Formation of such a charged species in benzene is unexpected, and as such we cannot exclude the sixth ligand being the neutral $NsNH_2$ amine donor (despite a better agreement between the calculated and experimental XAS pre-edge intensities for the $NsNH^-$ amido ligand). At this point, we cannot fully exclude formation of dinuclear complexes with ligand X being for example a bridging amido ligand. However, we consider this possibility less likely in view of the fact that similar XAS data were gathered for $3^{P2}{}_{Troc}$, which is based on the bulky porphyrin P2. No peak corresponding to a Co scatterer was observed in the EXAFS spectrum, which would be expected for a homodinuclear Co···Co species. It is further worth mentioning that the sixth ligand X (Figure 12) does not prevent conversion of mono-nitrene species $3^{P1}{}_{Ns}$ to bis-nitrene species $5^{P1}{}_{Ns}$ upon treatment with the strongly oxidizing *N*-nosyl iminoiodane 4_{Ns}. On adding an excess of 4_{Ns} to a solution of previously formed mono-nitrene species $3^{P1}{}_{Ns}$, clear EPR signals corresponding to bis-nitrene species $5^{P1}{}_{Ns}$ appeared, once again displaying the strongly oxidizing nature of *N*-nosyl iminoiodane. Apparently, the ligand X can be replaced or converted to a nosyl nitrene radical moiety upon reaction of mono-nitrene $3^{P1}{}_{Ns}$ with iminoiodane 4_{Ns}.

CONCLUSIONS

In conclusion, we have demonstrated that activation of both organic azides and iminoiodanes by cobalt(II) porphyrin complexes leads to formation of 'cobalt(III)-nitrene radical' complexes. Both species bear substantial spin density at the 'nitrene-moiety' and are key intermediates in cobalt-catalyzed nitrene transfer reactions. Notably, for the less bulky porphyrin complexes, the obtained species are markedly different. While organic azides generate predominantly mono-nitrene species, hypervalent iodine reagents such as iminoiodanes produce bis-nitrene species such as $5^{P1}{}_{Ns}$. This is the first report to demonstrate the formation of a bis-nitrene species of a cobalt porphyrin complex. The stronger oxidizing nature of the nitrene precursor 4_{Ns} is considered important to generate such species. The bis-nitrene species $5^{P1}{}_{Ns}$ has a markedly different electronic structure from the mono-nitrene species $3^{P1}{}_{Ns}$, $3^{P2}{}_{Ts}$, and $3^{P2}{}_{Troc}$ and also differs markedly from the electronic structure of the previously reported diamagnetic bis-imido Ru^{IV}-porphyrin species (por)$Ru^{VI}((=NR'')_2)$. Electronically, the mono- and the bis-nitrene species are markedly different; but XANES data for these species suggest that both are six-coordinate (O_h) complexes with similar averaged bond distances between cobalt(III) and the six N/O scatterers ($3^{P1}{}_{Ns}$: ∼1.95 Å; $5^{P1}{}_{Ns}$: ∼1.92 Å). The exact nature of the ligand X coordinated at the sixth available coordination site of the $[Co^{III}(por)(N^{\bullet}R'')]$ nitrene radical species $3^{P1}{}_{Ns}$, $3^{P2}{}_{Ts}$, and $3^{P2}{}_{Troc}$ remains speculative. For $3^{P1}{}_{Ns}$, the most probable candidates (based on a comparison between the experimental and DFT calculated Co K-edge XAS pre-edge intensities, complementary mass data, and the previously detected $NsND^{\bullet}$ radical) seem to be either the neutral NsNHD amine ligand or the anionic $NsND^-$ amido ligand.

The revelation of the presence of a sixth ligand even in the mono-nitrene species implies that the use of additives in such catalytic nitrene transfer reactions should not have a positive effect on the catalytic reactions. This is indeed seen to be the case in the earlier reports from the Zhang group, where additives have only a detrimental effect on catalysis if any (except for ee enhancement in one case but in lower yields).[39,40]

The two different types of catalytically relevant species detected are represented in Figure 12. Overall, these results signify the importance of the nature of nitrene sources in metal-catalyzed nitrene transfer processes. Depending on the nature of the nitrene precursor, the intermediates can be a result of a single oxidation of the catalyst at the metal center or a double oxidation where the second oxidation step occurs at the

DOI: 10.1021/jacs.5b01197
J. Am. Chem. Soc. 2015, 137, 5468−5479

porphyrin ring. In addition, the bis-nitrene species $5^{P1}{}_{Ns}$, though formed faster, lives shorter and is more reactive than the mono-nitrene species $3^{P1}{}_{Ns}$. Degradation of bis-nitrene species $5^{P1}{}_{Ns}$ occurs within hours after initial formation while decomposition of mono-nitrene species $3^{P1}{}_{Ns}$ is much slower (solutions of $3^{P1}{}_{Ns}$ in benzene-d_6 were stable for >24 h according to EPR and UV−vis). In addition, the studies described here clearly demonstrate the better performance of specially tailored cobalt(II) porphyrins like complex 1^{P2}, which not only give higher conversions to the nitrene-radical species but also help in preserving them for longer periods by the stabilizing effects of H-bonding between the catalyst amide arms and the nitrene moiety. The steric influence of the bulk in complex 1^{P2} also has an implication on the type of intermediates formed, as was shown for the reactions of 1^{P1} and 1^{P2} with *N*-nosyl iminoiodane 4_{Ns}. Detailed studies of the differences in reactivity between the mono- and bis-nitrene and implications in catalysis between these 'cobalt(III)-nitrene radical' species are a topic of current investigation and should shed new light on the catalytic mechanisms of nitrene transfer processes catalyzed by cobalt(II) porphyrin complexes.

■ ASSOCIATED CONTENT

Supporting Information

Experimental details, synthetic procedures, copies of NMR, MS, IR, VCD, EPR spectra, XANES/XAFS data, energies and geometries of stationary points (DFT), and supporting discussions. This material is available free of charge via the Internet at http://pubs.acs.org.

■ AUTHOR INFORMATION

Corresponding Authors

*b.debruin@uva.nl

*xpzhang@usf.edu

Author Contributions

$^{\nabla}$These authors contributed equally.

Notes

The authors declare no competing financial interest.

■ ACKNOWLEDGMENTS

We thank Ed Zuidinga (HIMS, UvA) for additional CSI-MS measurements, Dr. Erik R. Farquhar for help with XAS data collection, and Dr. Moniek Tromp for helpful discussions. The work was financially supported by the European Research Council (grant agreement 202886; BdB), The Netherlands Organization for Scientific Research (NWO-CW VICI grant 016.122.613, BdB), CMST COST Action CM1305 (ECOST-BIO), COST action STSM (COST-STSM-CM1305−21241), the University of Amsterdam (UvA), the National Science Foundation (CHE-1152767; X.P.Z.), the National Institutes of Health (R01-GM098777; X.P.Z.), and the "Solar Technologies Go Hybrid" initiative by the State of Bavaria (I.I.-B. and O.T.). K.R. acknowledges financial support from the Cluster of Excellence "Unifying Concepts in Catalysis" (EXC 314/1), Berlin. XAS data were obtained on NSLS beamline X3B (Brookhaven National Laboratory), with support from NIH grant P30-EB-009998 and the U.S. Department of Energy.

■ REFERENCES

(1) Godula, K.; Sames, D. *Science* **2006**, *312*, 67−72.
(2) Labinger, J. A.; Bercaw, J. E. *Nature* **2002**, *417*, 507−514.
(3) Shilov, A. E.; Shul, G. B. *Chem. Rev.* **1997**, *97*, 2879−2932.
(4) Doyle, M. P.; Forbes, D. C. *Chem. Rev.* **1998**, *98*, 911−935.
(5) Lu, H.-J.; Zhang, X. P. *Chem. Soc. Rev.* **2011**, *40*, 1899−1909.
(6) Davies, H. M. L.; Manning, J. R. *Nature* **2008**, *451*, 417−424.
(7) Davies, H. M. L. *Angew. Chem., Int. Ed.* **2006**, *45*, 6422−6425.
(8) Hili, R.; Yudin, A. K. *Nat. Chem. Biol.* **2006**, *2*, 284−287.
(9) Suarez, A. I. O.; Jiang, H.; Zhang, X. P.; de Bruin, B. *Dalton Trans.* **2011**, *40*, 5697−5705.
(10) Jin, L.-M.; Xu, X.; Lu, H.; Cui, X.; Wojtas, L.; Zhang, X. P. *Angew. Chem., Int. Ed.* **2013**, *52*, 5309−5313.
(11) Lu, H.; Subbarayan, V.; Tao, J.; Zhang, X. P. *Organometallics* **2010**, *29*, 389−393.
(12) Lu, H.; Hu, Y.; Jiang, H.; Wojtas, L.; Zhang, X. P. *Org. Lett.* **2012**, *14*, 5158−5161.
(13) Jin, L.; Lu, H.; Cui, Y.; Lizardi, C. L.; Arzua, T. N.; Wojtas, L.; Cui, X.; Zhang, X. P. *Chem. Sci.* **2014**, *5*, 2422−2427.
(14) Catino, A. J.; Nichols, J. M.; Forslund, R. E.; Doyle, M. P. *Org. Lett.* **2005**, *7*, 2787−2790.
(15) Shen, M.; Leslie, B. E.; Driver, T. G. *Angew. Chem., Int. Ed.* **2008**, *47*, 5056−5059.
(16) Stokes, B. J.; Dong, H.; Leslie, B. E.; Pumphrey, A. L.; Driver, T. G. *J. Am. Chem. Soc.* **2007**, *129*, 7500−7501.
(17) Espino, C. G.; Wehn, P. M.; Chow, J.; Du Bois, J.; V, S. U.; April, R. V.; H, C. *J. Am. Chem. Soc.* **2001**, *123*, 6935−6936.
(18) Shou, W. G.; Li, J.; Guo, T.; Lin, Z.; Jia, G. *Organometallics* **2009**, *28*, 6847−6854.
(19) Liang, J.; Yuan, S.; Huang, J.; Che, C.-M. *J. Org. Chem.* **2004**, *69*, 3610−3619.
(20) Fantauzzi, S.; Gallo, E.; Caselli, A.; Ragaini, F.; Casati, N.; Macchi, P.; Cenini, S. *Chem. Commun.* **2009**, 3952−3954.
(21) Abu-Omar, M. M. *Dalton Trans.* **2011**, *40*, 3435−3444.
(22) Zhang, J.; Hong Chan, P. W.; Che, C.-M. *Tetrahedron Lett.* **2005**, *46*, 5403−5408.
(23) Albone, D. P.; Aujla, P. S.; Taylor, P. C. *J. Org. Chem.* **1998**, *63*, 9569−9571.
(24) Clark, J. S.; Roche, C. *Chem. Commun.* **2005**, 5175−5177.
(25) Fructos, M. R.; Trofimenko, S.; Diaz-Requejo, M. M.; Perez, P. J. *J. Am. Chem. Soc.* **2006**, *128*, 11784−11791.
(26) Albone, D. P.; Challenger, S.; Derrick, A. M.; Fillery, S. M.; Irwin, J. L.; Parsons, C. M.; Takada, H.; Taylor, C.; Wilson, D. J. *J. Org. Biomol. Chem.* **2005**, 107−111.
(27) Liu, Y.; Che, C.-M. *Chem. - A Eur. J.* **2010**, *16*, 10494−10501.
(28) Chen, Y.; Ruppel, J. V.; Zhang, X. P. *J. Am. Chem. Soc.* **2007**, *129*, 12074−12075.
(29) Zhu, S.; Xu, X.; Perman, J. A.; Zhang, X. P. *J. Am. Chem. Soc.* **2010**, *132*, 12796−12799.
(30) Zhu, S.; Ruppel, J. V.; Lu, H.; Wojtas, L.; Zhang, X. P. *J. Am. Chem. Soc.* **2008**, *130*, 5042−5043.
(31) Zhu, S.; Perman, J. a; Zhang, X. P. *Angew. Chem., Int. Ed. Engl.* **2008**, *47*, 8460−8463.
(32) Li, Z.; Capretto, D. A.; Rahaman, R.; He, C. *Angew. Chem., Int. Ed.* **2007**, *46*, 5184−5186.
(33) Chang, J. W. W.; Chan, P. W. H. *Angew. Chem., Int. Ed.* **2008**, *47*, 1138−1140.
(34) Yang, J.; Weinberg, R.; Breslow, R. *Chem. Commun.* **2000**, 531−532.
(35) Chan, J.; Baucom, K. D.; Murry, J. A. *J. Am. Chem. Soc.* **2007**, *129*, 14106−14107.
(36) Liang, C.; Collet, F.; Robert-Peillard, F.; Müller, P.; Dodd, R. H.; Dauban, P. *J. Am. Chem. Soc.* **2008**, *130*, 343−350.
(37) Driver, T. G. *Org. Biomol.Chem.* **2010**, *8*, 3831−3846.
(38) Intrieri, D.; Zardi, P.; Caselli, A.; Gallo, E. *Chem. Commun.* **2014**, *50*, 11440−11453.
(39) Jones, J. E.; Ruppel, J. V.; Gao, G.; Moore, T. M.; Zhang, X. P. *J. Org. Chem.* **2008**, *73*, 7260−7265.
(40) Gao, G.; Jones, J. E.; Vyas, R.; Harden, J. D.; Zhang, X. P. *J. Org. Chem.* **2006**, *71*, 6655−6658.
(41) Subbarayan, V.; Ruppel, J. V.; Zhu, S.; Perman, J. A.; Zhang, X. P. *Chem. Commun.* **2009**, 4266−4268.

DOI: 10.1021/jacs.5b01197
J. Am. Chem. Soc. 2015, 137, 5468−5479

(42) Ruppel, J. V.; Jones, J. E.; Huff, C. A.; Kamble, R. M.; Chen, Y.; Zhang, X. P. *Org. Lett.* **2008**, *10*, 1995−1998.
(43) Lyaskovskyy, V.; Suarez, A. I. O.; Lu, H.; Jiang, H.; Zhang, X. P.; de Bruin, B. *J. Am. Chem. Soc.* **2011**, 12264−12273.
(44) Luca, O. R.; Crabtree, R. H. *Chem. Soc. Rev.* **2013**, *42*, 1440−1459.
(45) Lyaskovskyy, V.; de Bruin, B. *ACS Catal.* **2012**, *2*, 270−279.
(46) Van der Vlugt, J. I. *Eur. J. Inorg. Chem.* **2012**, *2012*, 363−375.
(47) Pierpont, C. G.; Buchanan, R. M. *Coord. Chem. Rev.* **1981**, *38*, 45−87.
(48) Kaim, W.; Schwederski, B. *Coord. Chem. Rev.* **2010**, *254*, 1580−1588.
(49) Boyer, J. L.; Rochford, J.; Tsai, M.-K.; Muckerman, J. T.; Fujita, E. *Coord. Chem. Rev.* **2010**, *254*, 309−330.
(50) Lever, A. B. P. *Coord. Chem. Rev.* **2010**, *254*, 1397−1405.
(51) Jones, G. D.; Martin, J. L.; Mcfarland, C.; Allen, O. R.; Hall, R. E.; Haley, A. D.; Brandon, R. J.; Konovalova, T.; Desrochers, P. J.; Pulay, P.; Vicic, D. A. *J. Am. Chem. Soc.* **2006**, *128*, 13175−13183.
(52) Ciszewski, J. T.; Mikhaylov, D. Y.; Holin, K. V.; Kadirov, M. K.; Budnikova, Y. H.; Sinyashin, O.; Vicic, D. A. *Inorg. Chem.* **2011**, *50*, 8630−8635.
(53) Scarborough, C. C.; Lancaster, K. M.; DeBeer, S.; Weyhermüller, T.; Sproules, S.; Wieghardt, K. *Inorg. Chem.* **2012**, *51*, 3718−3732.
(54) Tejel, C.; Ciriano, M. A.; del Rio, M. P.; van den Bruele, F. J.; Hetterscheid, D. G. H.; Tsichlis i Spitas, N.; de Bruin, B. *J. Am. Chem. Soc.* **2008**, *130*, 5844−5845.
(55) Tejel, C.; Asensio, L.; del Río, M. P.; de Bruin, B.; López, J. A.; Ciriano, M. A. *Angew. Chem., Int. Ed.* **2011**, *50*, 8839−8843.
(56) Lu, C. C.; Bill, E.; Weyhermüller, T.; Bothe, E.; Wieghardt, K. *J. Am. Chem. Soc.* **2008**, *130*, 3181−3197.
(57) de Bruin, B.; Bill, E.; Bothe, E.; Weyhermüller, T.; Wieghardt, K. *Inorg. Chem.* **2000**, *39*, 2936−2947.
(58) Chirik, P. J.; Wieghardt, K. *Science* **2010**, *327*, 794−795.
(59) Tondreau, A. M.; Milsmann, C.; Patrick, A. D.; Hoyt, H. M.; Lobkovsky, E.; Wieghardt, K.; Chirik, P. J. *J. Am. Chem. Soc.* **2010**, *132*, 15046−15059.
(60) Intermolecular, I.; Russell, S. K.; Lobkovsky, E.; Chirik, P. J. *J. Am. Chem. Soc.* **2011**, *133*, 8858−8861.
(61) Bouwkamp, M. W.; Bowman, A. C.; Lobkovsky, E.; Chirik, P. J. *J. Am. Chem. Soc.* **2006**, *128*, 13340−13341.
(62) Dzik, W. I.; Zhang, X. P.; de Bruin, B. *Inorg. Chem.* **2011**, *50*, 9896−9903.
(63) Dzik, W. I.; Xu, X.; Zhang, X. P.; Reek, J. N. H.; de Bruin, B. *J. Am. Chem. Soc.* **2010**, *132*, 10891−10902.
(64) Lu, H.; Dzik, W. I.; Xu, X.; Wojtas, L.; de Bruin, B.; Zhang, X. P. *J. Am. Chem. Soc.* **2011**, *133*, 8518−8521.
(65) Suarez, A. I. O; Lyaskovskyy, V.; Reek, J. N. H.; van der Vlugt, J. I.; de Bruin, B. *Angew. Chem., Int. Ed.* **2013**, *52*, 12510−12529.
(66) Liu, Y.; Guan, X.; Wong, E. L.; Liu, P.; Huang, J.; Che, C. *J. Am. Chem. Soc.* **2013**, *135*, 7194−7204.
(67) Kundu, S.; Miceli, E.; Farquhar, E.; Pfaff, F. F.; Kuhlmann, U.; Hildebrandt, P.; Braun, B.; Greco, C.; Ray, K. *J. Am. Chem. Soc.* **2012**, *134*, 14710−14713.
(68) Lu, H.; Tao, J.; Jones, J. E.; Wojtas, L.; Zhang, X. P. *Org. Lett.* **2010**, *12*, 1248−1251.
(69) Au, S.; Huang, J.; Yu, W.; Fung, W.; Che, C.-M. *J. Am. Chem. Soc.* **1999**, *121*, 9120−9132.
(70) Leung, S. K.; Tsui, W.; Huang, J.; Che, C.; Liang, J.; Zhu, N. *J. Am. Chem. Soc.* **2005**, *127*, 16629−16640.
(71) Guo, Z.; Guan, X.; Huang, J.-S.; Tsui, W.-M.; Lin, Z.; Che, C.-M. *Chem.—Eur. J.* **2013**, *19*, 11320−11331.
(72) Law, S.-M.; Chen, D.; Chan, S. L.-F.; Guan, X.; Tsui, W.-M.; Huang, J.-S.; Zhu, N.; Che, C.-M. *Chem.—Eur. J.* **2014**, *20*, 11035−11047.
(73) Manca, G.; Gallo, E.; Intrieri, D.; Mealli, C. *ACS Catal.* **2014**, *4*, 823−832.
(74) See for example: Nam, W. *Acc. Chem. Res.* **2007**, *40*, 522−531 and references therein.
(75) The quartet-doublet gap might be underestimated, as hybrid functionals often overestimate the stability of higher-spin states: Swart, M. *J. Chem. Theory Comput.* **2008**, *4*, 2057−2066.
(76) Campo Dall' Orto, V.; Carballo, R.; Hurst, J. A.; Rezzano, I. *Spectrochim. Acta, Part A* **2005**, *61*, 2089−2093.
(77) Mu, X. H.; Kadish, K. M. *Inorg. Chem.* **1989**, *28*, 3743−3747.
(78) Lin, X. Q.; Kadish, K. M. *Inorg. Chem.* **1986**, *25*, 3242−3248.
(79) Dey, S.; Ikbal, S. A.; Rath, S. P. *New J. Chem.* **2014**, *38*, 1458−1470.
(80) Gasyna, Z.; Stillman, M. J. *Inorg. Chem.* **1990**, *29*, 5101−5109.
(81) Gasyna, Z.; Browett, W. R.; Stillman, M. J. *Inorg. Chem.* **1988**, *27*, 4619−4622.
(82) Yu, R. P.; Darmon, J. M.; Milsmann, C.; Margulieux, G. W.; Stieber, S. C. E.; DeBeer, S.; Chirik, P. J. *J. Am. Chem. Soc.* **2013**, *135*, 13168−13184.
(83) Tomson, N. C.; Crimmin, M. R.; Petrenko, T.; Rosebrugh, L. E.; Sproules, S.; Boyd, W. C.; Bergman, R. G.; DeBeer, S.; Toste, F. D.; Wieghardt, K. *J. Am. Chem. Soc.* **2011**, *133*, 18785−18801.

DOI: 10.1021/jacs.5b01197
J. Am. Chem. Soc. 2015, 137, 5468−5479